PERGAMON

International Journal of Heat and Mass Transfer 45 (2002) 1017–1031

International Journal of HEAT and MASS TRANSFER

www.elsevier.com/locate/ijhmt

Thermophysical properties of high porosity metal foams

A. Bhattacharya, V.V. Calmidi [1], R.L. Mahajan *

Mechanical Engineering Department, Engineering Center, University of Colorado at Boulder, Campus Box 427, Boulder, CO 80309-0427, USA

Received 27 December 2000; received in revised form 30 June 2001

Abstract

In this paper, we present a comprehensive analytical and experimental investigation for the determination of the effective thermal conductivity (k_e), permeability (K) and inertial coefficient (f) of high porosity metal foams. In the first part of the study, we provide an analysis for estimating the effective thermal conductivity (k_e). Commercially available metal foams form a complex array of interconnected fibers with an irregular lump of metal at the intersection of two fibers. In our theoretical model, we represent this structure by a model consisting of a two-dimensional array of hexagonal cells where the fibers form the sides of the hexagons. The lump is taken into account by considering a circular blob of metal at the intersection. The analysis shows that k_e depends strongly on the porosity and the ratio of the cross-sections of the fiber and the intersection. However, it has no systematic dependence on pore density. Experimental data with aluminum and reticulated vitreous carbon (RVC) foams, using air and water as fluid media are used to validate the analytical predictions.

The second part of our paper involves the determination of the permeability (K) and inertial coefficient (f) of these high porosity metal foams. Fluid flow experiments were conducted on a number of metal foam samples covering a wide range of porosities and pore densities in our in-house wind tunnel. The results show that K increases with pore diameter and porosity of the medium. The inertial coefficient, f, on the other hand, depends only on porosity. An analytical model is proposed to predict f based on the theory of flow over bluff bodies, and is found to be in excellent agreement with the experimental data. A modified permeability model is also presented in terms of the porosity, pore diameter and tortuosity of our metal foam samples, and is shown to be in reasonable agreement with measured data. © 2002 Published by Elsevier Science Ltd.

1. Introduction

Convective transport in porous media has been studied extensively for over 150 years now, see [1–5] for excellent reviews on this subject. Majority of the studies reported in literature deal with naturally occurring low porosity media such as packed beds and granular media. For these, ε varies from 0.3 to 0.6. The subject matter of this paper is high porosity fibrous metal foams for which $\varepsilon > 0.9$. For these types of media, the published studies are relatively few.

Fig. 1(a) shows a picture of the metal foam. It has an open-celled structure composed of dodecahedron-like cells (Fig. 1(b)), which have 12–14 pentagonal or hexagonal faces. The edges of these cells are composed of metal fibers and, typically, there is a lumping of solid material at the intersection of fibers. The fibrous matrix is made of aluminum alloy T-6201, which has a thermal conductivity of 218 W/m K. Two quantities, the porosity (ε) and the pore density are used to describe the porous medium, where the latter is typically expressed in units of pores per inch (PPI). The cross-section of the metal fiber is a function of porosity, and changes from a circle at $\varepsilon = 0.85$ to an inner concave triangle at $\varepsilon = 0.97$ [6,7].

Calmidi [6] proposed an open cell representation, as shown in Fig. 1(b), to approximate the metal foam structure. It is shaped as a cube of unit volume, with

* Corresponding author. Tel.: +1-303-492-0481; fax: +1-303-492-3498.

E-mail address: mahajan@spot.colorado.edu (R.L. Mahajan).

[1] Present address: IBM, 1701, North Street, Endicott, NY 13760, USA.

0017-9310/02/$ - see front matter © 2002 Published by Elsevier Science Ltd.
PII: S0017-9310(01)00220-4

Nomenclature

a	length scale for a dodecahedron; coefficient for curve fit equations (kg/m^3 s)
A	correlation constant for thermal conductivity; cross-sectional area (m^2)
b	coefficient for curve fit equations (kg/m^4)
C_D	form drag coefficient
d	distance between thermocouples in the insulation (m); diameter (m)
f	inertial coefficient
G	geometric function
H	height of the foam sample used for thermal conductivity measurements (m)
K	permeability (m^2)
k	thermal conductivity (W/m K)
l	half length of each side of hexagonal intersection (m)
L	half length of fiber (m); length of metal foam samples for pressure drop (m)
N	number of fibers in x or y direction in the z-plane in the unit cube, Fig. 1(b)
P	pressure (N/m^2)
Q	rate of heat input (W)
Q_{loss}	rate of heat loss from the top and sides (W)
R	radius of the circular intersection (m)
r	geometric parameter, t/R
S	shape function, Eq. (26)
t	half thickness of fiber (m)
T	temperature (K)
u	velocity (m/s)
V	volume (m^3)
y	characteristic length in the thermal conductivity model (m)

Greek symbols

Δ	difference
ρ	density of fluid (kg/m^3)
μ	viscosity of fluid (N/m s)
ε	porosity
θ	effective angle of inclination of fiber
χ	tortuosity, Eq. (18)

Subscripts

∞, amb	ambient
1, 2	refers to the characteristic lengths in the thermal conductivity model
c	cross-section
e	effective
f	fiber (for diameter), fluid
gr	thermal grease
I, II, III, IV, V	refers to the different layers in the thermal conductivity model
m	metal foam
p	pore
s	solid
sf	solid–fluid
st	Styrofoam
tot	total

porosity ε, with N^2 fibers of diameter d_f and N^2 pores of diameter d_p in each of the x, y, z directions. Thus, for a giving porosity ε, we can represent the total solid volume of the cube as

$$3N^2 \times \frac{\pi d_f^2}{4} \times 1 = (1-\varepsilon) \times 1^3.$$

Further, noting that $N = 1/d_p$, we obtain

$$\frac{d_f}{d_p} = 2\sqrt{\frac{1-\varepsilon}{3\pi}}\frac{1}{G}, \tag{1}$$

where G is a shape function that takes into account the variation of fiber cross-section with porosity [6,7] and is given by $G = 1 - e^{-(1-\varepsilon)/0.04}$.

Next, we modify Eq. (1) to reflect the difference between the open cell representation and the three-dimensional dodecahedron structure. First, d_p in Eq. (1) should be replaced by the characteristic cell size, a, which can be determined by counting the number of cells in a given length of foam and repeating the procedure over different lengths to get an average value. Further, for the orientation in Fig. 1(b), it can be shown that of the 30 edges, 10 edges are inclined at an angle $\alpha = 0°$, 10 at an angle $\beta = 58.27°$, and 10 at an angle $\gamma = 31.72°$ to the horizontal. The distance, a, between two parallel pentagons is, thus, given by

$$a = (2\sin 58.27° + \sin 31.72°)l = 2.23l, \tag{2}$$

where l is the length of one side of the pentagon. Next, the equivalence between the two structures is achieved by assuming that the square face formed by the cylinders has the same area as the pentagonal face formed by the fibers in the dodecahedron. Since the interior angle of a regular pentagon is 108°, its area can be written as

$$A = 5\left[0.5l\left(\frac{l}{2}\tan\frac{108°}{2}\right)\right] = 1.72l^2 = 0.35a^2 \tag{3}$$

(using Eq. (2)). Equating this to the area of a square face of the cube, having side d_p, we get $d_p = \sqrt{0.35a^2} = 0.59a$. Using this result in Eq. (1) and replacing a by d_p we get

$$\frac{d_f}{d_p} = 1.18\sqrt{\frac{1-\varepsilon}{3\pi}}\frac{1}{G}. \tag{4}$$

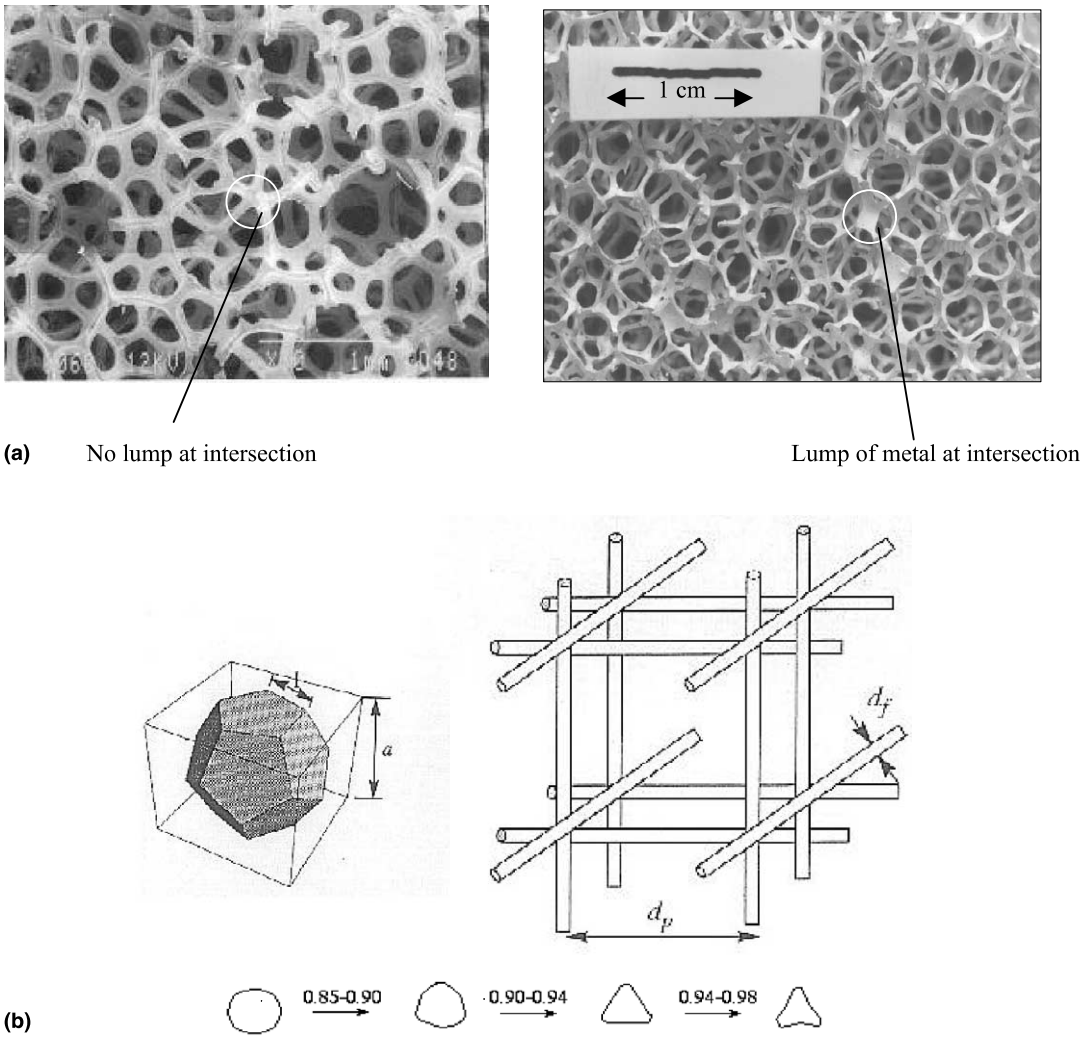

Fig. 1. (a) Samples used in [52] (left) and present study (right). (b) Open cell representation of metal foam and schematics of the fiber cross-sections at different porosities.

The pore diameter obtained is thus a function of porosity and pore density for each sample. Calmidi [6] found Eq. (4) to match the measured values of d_f and d_p to within $\pm 7\%$.

High porosity metal foams have long been used in design of aircraft wing structure in the aerospace industry, catalytic surfaces for chemical reactions, core structure for high strength panels, and containment matrix and burn rate enhancer for solid propellants. More recently, they have been considered as potential candidates for heat sinks and compact heat exchangers. These applications, however, require characterization of these materials for fluid flow and heat transfer. Central to this requirement is the need for accurate evaluation of its transport properties, e.g. effective thermal conductivity, permeability and inertial coefficient. The research reported in this paper was undertaken to fulfill this need.

2. Effective thermal conductivity

2.1. Introduction

Heat conduction in fully saturated porous matrices has been studied in detail over the years by many researchers [8–21] and has been summarized in a number of excellent review articles, the most recent being authored by Kaviany [2], Nield and Bejan [4], Whitaker [22], Cheng and Hsu [23], and Hsu [24].

Mantle and Chang [25] reviewed the earlier studies on thermal conductivity of fibrous materials [26–30],

mostly pertaining to wicking materials in heat pipes, and presented a generalized empirical model based on the experimental data by Semena and Zaripov [29]. They took into account the effects of the thermal conductivity of the constituent solid and fluid media, porosity and l/d ratio of the fibers. Pertinent to high porosity metal foams, Calmidi and Mahajan [31] presented a one-dimensional heat conduction model considering the porous medium to be formed of a two-dimensional array of hexagonal cells (Fig. 2(a)). The irregularly shaped lump of metal at the intersection of two fibers was represented as a square 'blob' of metal at the intersection of two sides of a hexagon. Their model, however, involved an unknown parameter 'r', which had to be determined by fitting their model to experimental data. To this end, they conducted experiments on aluminum foams of different porosity and PPI using air and water as the fluid media and found $r = 0.09$. Further, the model had only a two-fold rotational symmetry because of square intersections in a hexagonal array. Paek et al. [32] reported their experimental results on thermal conductivity of aluminum foams in air. Their experimental data matched very well with those of Calmidi and Mahajan [31]. Recently, Boomsma and Poulikakos [33] proposed a three-dimensional model of the metal foam structure in the form of tetrakaidecahedral cells with cubic nodes at the intersection of two fibers. Similar to Calmidi and Mahajan [31], their model also involved a geometric parameter that was evaluated using the experimental data reported in [31].

In this research, we extend the analysis of Calmidi and Mahajan [31] to develop a model with a circular intersection, which results in a six-fold rotational symmetry. The value of r is determined from physical measurements under a microscope and compared with model predictions. New experimental data are also presented for a wider range of k_s/k_f values using foams of reticulated vitreous carbon (RVC) with air and water as the fluid media. Finally, a new empirical correlation, in terms of the effective thermal conductivities in 'series' and 'parallel' arrangement of the fluid and solid phases is presented.

2.2. Analytical model

The analytical model of Calmidi and Mahajan [31] is modified to replace the square intersection by a circular one. The unit cell (Fig. 2(b)), in this case, consists of five different layers in series. In each layer, the solid and fluid phases are in parallel. The thermal conductivity of the layers can be individually written as:

$$k_{\mathrm{I}} = k_{\mathrm{f}} + \frac{(k_{\mathrm{s}} - k_{\mathrm{f}})}{3Lt}\left(Lt + \frac{R^2}{2}\left(\sin^{-1}\frac{t}{R} + \frac{t}{R}\sqrt{1 - \frac{t^2}{R^2}}\right)\right), \quad (5)$$

$$k_{\mathrm{II}} = k_{\mathrm{f}} + \frac{(k_{\mathrm{s}} - k_{\mathrm{f}})R^2}{\frac{3L}{2}\left(\sqrt{3(R^2 - t^2)} - 3t\right)}\left[\sin^{-1}\left(\frac{1}{2R}\left(\sqrt{3(R^2 - t^2)} - t\right)\right) - \sin^{-1}\left(\frac{t}{R}\right) + \frac{1}{2}\sin 2\left(\sin^{-1}\left(\frac{1}{2R}\left(\sqrt{3(R^2 - t^2)} - t\right)\right)\right) - \frac{1}{2}\sin 2\left(\sin^{-1}\left(\frac{t}{R}\right)\right)\right], \quad (6)$$

$$k_{\mathrm{III}} = k_{\mathrm{f}} + \frac{(k_{\mathrm{s}} - k_{\mathrm{f}})}{3Lt}\left(Rt + \frac{R^2}{2}\left(\sin^{-1}\frac{y_2}{R} - \sin^{-1}\frac{y_1}{R} + \frac{1}{2}\sin 2\left(\sin^{-1}\frac{y_2}{R}\right) - \frac{1}{2}\sin 2\left(\sin^{-1}\frac{y_1}{R}\right)\right) + \frac{\sqrt{3}}{2}\frac{y_2^2 - y_1^2}{2} - \frac{\sqrt{3}}{2}y_1 t\right), \quad (7)$$

$$k_{\mathrm{IV}} = k_{\mathrm{f}} + \frac{(k_{\mathrm{s}} - k_{\mathrm{f}})}{3L(R - y_2)}\left(R^2\left(\frac{\pi}{2} - \sin^{-1}\frac{y_2}{R}\right) - \frac{R^2}{2}\sin 2\left(\sin^{-1}\frac{y_2}{R}\right) + \frac{4t}{\sqrt{3}}(R - y_2)\right), \quad (8)$$

$$k_{\mathrm{V}} = k_{\mathrm{f}} + (k_{\mathrm{s}} - k_{\mathrm{f}})\frac{4t}{3\sqrt{3}L}. \quad (9)$$

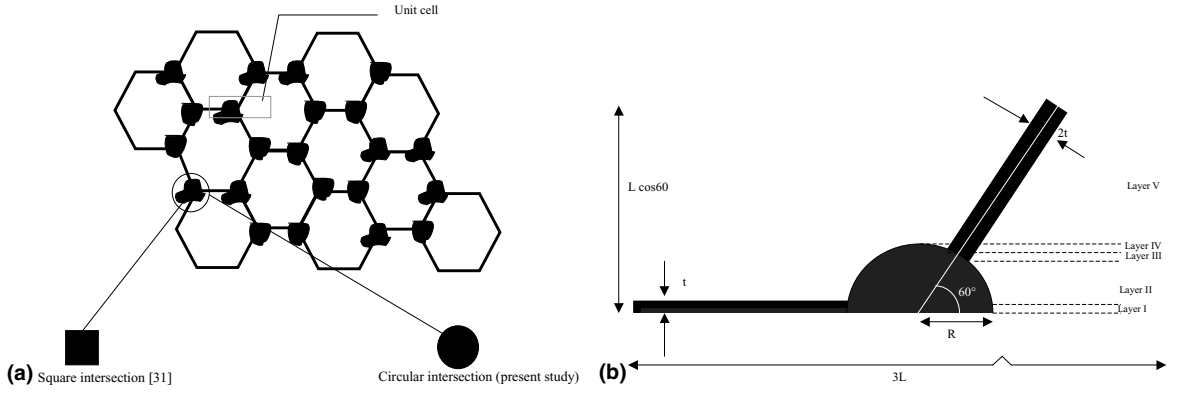

Fig. 2. (a) Analytical for thermal conductivity. (b) Unit cell for the circular intersection.

Here $R=$radius of the circular intersection, $y_1=\frac{1}{2}(\sqrt{3(R^2-t^2)}-t)$ and $y_2=\frac{1}{2}(\sqrt{3(R^2-t^2)}+t)$.

The effective thermal conductivity, k_e, is then simply the thermal conductivities of the individual layers in series. Noting that R/L can be expressed in terms of porosity using $\varepsilon=1-(V_s/V_{tot})$, the only unknown in Eqs. (5)–(9) is $r=t/R$, which needs to determined.

It is clear from the equations above that the size of the intersection plays a significant role in determining k_e. In the limiting case when the size of the intersection goes to zero (which implies $r\to\infty$), the effective thermal conductivity can be obtained from the model equations by setting $R=0$. The resulting expression is

$$k_e=\left(\left(\frac{2}{\sqrt{3}}\right)\left(\frac{t/L}{k_f+\frac{(k_s-k_f)}{3}}+\frac{\frac{\sqrt{3}}{2}-\left(\frac{t}{L}\right)}{k_f}\right)\right)^{-1},$$

where (10)

$$\frac{t}{L}=\frac{-\sqrt{3}-\sqrt{3+(1-\varepsilon)\left(\sqrt{3}-5\right)}}{1+\frac{1}{\sqrt{3}}-\frac{8}{3}}.$$

2.3. Determination of 'r'

As mentioned earlier in Eqs. (5)–(9) for k_e, the only unknown is r. As a first approximation, we took a number of physical measurements from pictures taken under a microscope to get an estimate of r. The measurements showed the value of r to fall between 0.17 and 0.21, with an average value of about 0.19. Details of these measurement values can be found in [34].

To test the validity of the model and fine tune the value of r, experiments were conducted with foams of RVC using air and water as the fluid media. A schematic of the experimental set-up is shown in Fig. 3(a). The set-up consisted of a test specimen sandwiched between two highly conducting copper plates. The specimens were 7.5 cm × 7.5 cm × 4.38 cm. The larger dimensions in the lateral direction ensured small lateral losses. To minimize contact resistance, a thin layer of thermal grease ($k_{gr}\sim 2$ W/m K) was applied between the copper plates and the sample. Four 0.127 mm, T-type thermocouples were attached to each of the two copper plates at points of varying distance from the center as shown in the figure. The thermocouples were connected to a data acquisition system. The top plate was heated by using four patch heaters of known power, which were connected to a DC power supply. The lower plate was cooled by a constant temperature bath in a plexiglass tank maintained by flowing water from a re-circulating water chiller at 5 °C. The whole assembly was housed in a plexiglass enclosure and insulated on the four sides and the top by low conductivity Styrofoam ($k_{st}=0.029$ W/m K at 25 °C). The plexiglass housing for the sample was provided with a small tap for filling with different fluids. Thermocouples were also embed-

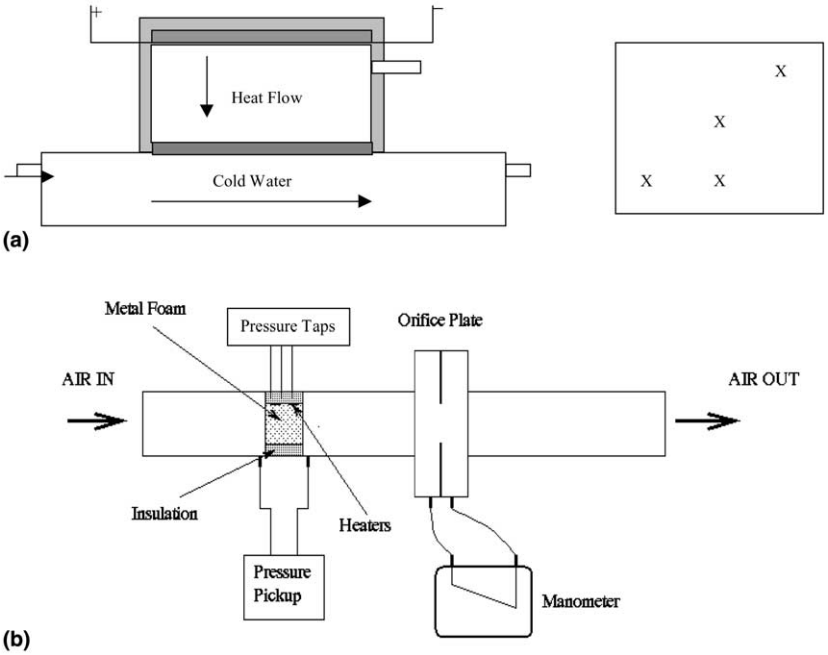

Fig. 3. (a) Schematic of the experimental set-up for thermal conductivity measurements and thermocouple positions. (b) Schematic of the experimental set-up used for pressure drop measurements.

ded in the Styrofoam insulation to estimate lateral heat losses as well as heat loss from the top.

Following the experimental procedure of Calmidi and Mahajan [31], the steady-state readings were taken for the temperature difference between the hot and cold plates. The procedure was repeated three times for each sample. The variability was found to be less than 2% in all the cases. The lateral losses and losses from the top were calculated using the steady-state readings of the thermocouples embedded in the insulation. The losses can be estimated using $Q_{\text{loss}} = k_{\text{st}} A_{\text{c}} (\Delta T/d)$. Knowing Q and Q_{loss}, we can then write

$$k_{\text{e}} = (Q - Q_{\text{loss}}) \frac{H}{A_{\text{m}} \Delta T}. \tag{11}$$

In order to check the accuracy of the loss estimates, a two-dimensional finite element heat conduction model (for details, see [34,35]) was simulated using the FEM software MARC$^{\text{TM}}$ [36]. The dimensions of the sample and the insulation as well as the boundary conditions at the hot and cold plates were specified to correspond to the experimental set-up. At the lateral sides, a heat transfer co-efficient of 5 W/m^2 K and an ambient temperature of 25 °C were specified. The thermal conductivities of the samples were assigned using Eq. (11). From the heat flux contours in the horizontal and vertical directions, the calculated values of heat loss from the sides and the top were found to be very close to our estimates using the one-dimensional heat conduction approximation. The conclusion is that for the given experimental conditions, a one-dimensional heat conduction approximation is accurate for calculating the losses.

The measured effective thermal conductivities of the foams are listed in Table 1 and are plotted in Fig. 4(a). The past experimental data of Calmidi and Mahajan [31] for Al–air and Al–water combinations are also plotted. We first note from the tabulated data that there is no systematic dependence of k_{e} on pore density. Earlier research by Mantle and Chang [25], and Semena and Zaripov [29] have also shown that for porosities of the order of 90% or higher, the effect of pore density on the effective thermal conductivity of the porous medium is negligible. Thus our conclusion is consistent with these prior observations as well as with the experimental results of Calmidi and Mahajan [31] and Paek et al. [32]. Next, we note from Fig. 4(a) that the predictions of our model are in excellent agreement with the experimental data covering a large range of $k_{\text{s}}/k_{\text{f}}$ ratios. A clear conclusion is that our model can generally be used for high porosity media, including the commercially available metal foam samples, if the value of r can be accurately evaluated. For an ordered medium, the value can be determined from measurements. However, in case of random media like these fibrous foams, taking physical measurements can be relatively difficult. In such cases, an alternative approach is to use experimental data to determine r in our model, as followed by Calmidi and Mahajan [31].

To quantify the effect of intersection, we next compared our experimental data with the predictions of Eq. (10) derived for $r \to \infty$. For a given porosity, the experimentally determined values of k_{e} were almost 50% of the analytical predictions. This is because the final inclined fiber layer contributes the most to the thermal resistance. In the presence of the intersection, the cross-sectional area (thickness) of the fiber decreases due to lumping of metal at the intersection, which results in an increase in the thermal resistance. Even though the resistance due to the horizontal layer (layer I) increases for the same reason, the intersection itself introduces an additional thermal resistance, which contributes to lowering of the effective thermal conductivity. An implication of the above analysis is that for a given porosity and pore density, it is desirable to manufacture

Table 1
Effective thermal conductivity of aluminum and RVC foams

PPI	Porosity	Al–air (W/m K)	Al–water (W/m K)	RVC–air (W/m K)	RVC–water (W/m K)
5	0.971	2.7	3.7		
5	0.9664			0.164	0.73
5	0.946	4.6	5.4		
5	0.905	6.7	7.65		
10	0.9724			0.15	0.722
10	0.949	3.9	4.8		
10	0.909	6.7	7.6		
20	0.978	2.2	3.05		
20	0.9615			0.17	0.743
20	0.949	4	4.95		
20	0.906	6.9	7.65		
40	0.972	2.5	3.3		
40	0.9681			0.16	0.727f
40	0.952	3.9	4.75		
40	0.937	4.5	5.35		

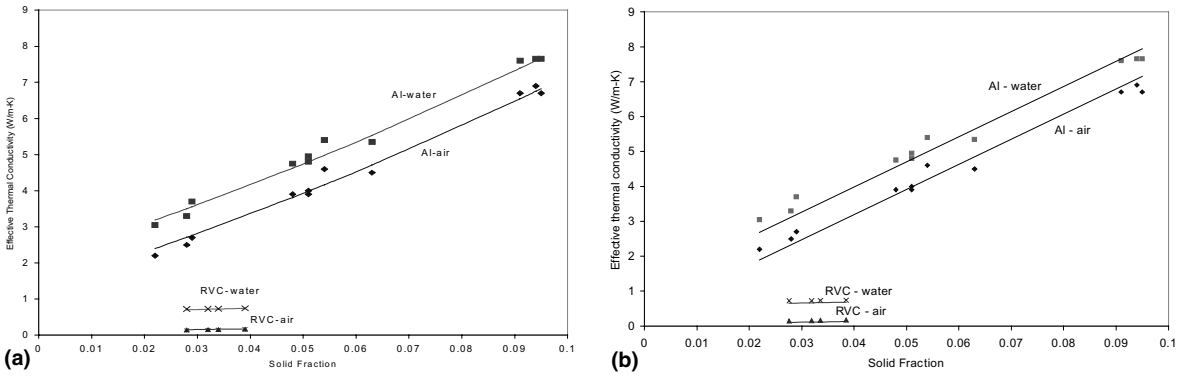

Fig. 4. (a) Experimental data (symbols) vs. model predictions (lines) for circular intersection ($r = 0.19$). (b) Experimental data (symbols) vs. empirical correlation (lines) predictions (Eq. (13)).

these foams without the metal intersection (or with minimal intersection size) for higher heat dissipation.

Zumbrunnen et al. [37,38] developed a thermal conductance model for porous solids using a probabilistically determined unit cell for a characteristic geometry. The model involved a parameter ϕ, which had to be determined empirically. Experiments were conducted on firebrick, alumina and zirconia insulations, and ceramic foams to determine the values of ϕ for the respective porous media. The model predictions matched well with the experimental data. When applied to our experimental results, good agreement was found for ϕ values of 0.042, 0.82, 1.11 and 5.47 for Al–air, Al–water, RVC–air and RVC–water, respectively. Thus the value of ϕ in their model is dependent on the composition of the porous medium. In comparison, the value of r in our model is purely a geometric parameter and is independent of the solid–fluid combination.

2.4. Error analysis

The main uncertainties in this experiment are due to errors in measurements of power, physical dimensions and thermocouple readings and those due to conduction losses through the thermocouples. The maximum error in the multimeter readings for the voltage and resistance measurements is 0.5% (manufacturer's data sheet). This results in an error of 1.5% in the estimation of the heat input Q. The combined error (resolution of the data acquisition unit, thermocouple calibration) in the estimation of the temperature difference under the given conditions is 0.2 °C. The temperature differences observed in our experiments were of the order of 30 °C. The error in measurement is thus 0.67%. The effective thermal conductivity of the RVC samples in all the cases (highest values being 0.17 W/m K for RVC–air and 0.743 W/m K for RVC–water) is lower than the thermal conductivity of the thermal grease ($k_{gr} \sim 2$ W/m K) used in the experiments. Hence, contact resistance can be neglected. In case of the aluminum samples of Calmidi and Mahajan [31], the foam samples were brazed on to the hot and cold plates to give minimal contact resistance. The application of the thin layer of thermal grease, however, can give rise to an error in the measurement of the sample thickness. For a sample thickness of 43.75 mm., this error is 0.75%. Similarly, the error in measurement of the cross-sectional area can be estimated to be 0.75%. The heat losses through the Styrofoam insulation were accounted for as discussed before, while the conduction losses through the thin thermocouple wires (diameter of 0.127 mm) were very small and hence neglected. Based on the preceding errors, the total error in the measurement of the effective thermal conductivity can be calculated using [39]

$$\frac{\Delta k_e}{k_e} = \sqrt{\left(\frac{\Delta Q}{Q}\right)^2 + \left(\frac{\Delta L_m}{L_m}\right)^2 + \left(\frac{\Delta A_m}{A_m}\right)^2 + \left(\frac{\Delta(\Delta T)}{\Delta T}\right)^2} \tag{12}$$

and was found to be ±3.8%.

2.5. Empirical correlation

In this section, we present an empirical correlation for easy estimation of the effective thermal conductivity of these fibrous foams based on the experimental data for RVC foams discussed above and the data for aluminum foams obtained by Calmidi and Mahajan [31]. The two limiting values of k_e for a porous medium are given by

$$k_e = \varepsilon k_f + (1-\varepsilon)k_s \quad \text{and} \quad k_e = \frac{1}{\frac{\varepsilon}{k_f} + \frac{1-\varepsilon}{k_s}}.$$

The former represents the upper limit with the solid and fluid phases arranged in parallel to the direction to the heat flow path, while the latter corresponds to the lower limit with the two phases arranged in series. The effective

thermal conductivity of a random porous medium can be conceived of being comprised of contributions from both these two limiting values. Based on the above argument we propose an empirical correlation of the form

$$k_e = A(\varepsilon k_f + (1-\varepsilon)k_s) + \frac{1-A}{\left(\frac{\varepsilon}{k_f} + \frac{1-\varepsilon}{k_s}\right)}. \quad (13)$$

This satisfies both the limits when $\varepsilon = 0$ (solid) and $\varepsilon = 1$ (fluid). The best fit for all the data was found for $A = 0.35$ with an overall R^2 value of 0.97. The plots of the experimental data along with correlation are shown in Fig. 4(b).

3. Determining permeability (K) and inertial coefficient (f)

3.1. Introduction

Following the earlier formulations by Darcy [40] and Forchheimer [41], the following Forchheimer extended Darcy's equation is widely accepted for steady-state, unidirectional pressure drop in a homogeneous, uniform, and isotropic porous medium, fully saturated with a Newtonian incompressible fluid [42–45]

$$-\frac{dp}{dx} = \frac{\mu u}{K} + \frac{\rho f}{\sqrt{K}}u^2. \quad (14)$$

Both K and f are strongly related to the structure of the medium. Over the years, several studies have been dedicated to the determination of these two parameters [46–51].

For high porosity media, one of the earliest cited research is that of Beavers and Sparrow [42]. They quantified pressure drop in nickel foams and concluded that $f = 0.074$. Subsequent studies by Vafai and Tien [43], Antohe et al. [45], Du Plessis et al. [52], Lage et al. [53] and Paek et al. [32] found this estimate of f to be incorrect. Vafai and Tien [43] measured K and f for 'Foametal' and found the values of K and f as 1.11×10^{-7} m^2 and 0.057, respectively. Antohe et al. [45] measured K and f for compressed metal foams ($\varepsilon \sim 0.3$–0.7) but did not correlate their results. Du Plessis et al. [52] derived a model for fluid flow in metal foams based on a periodic unit cell representation for metal foams. Their study was based on experimental data for samples of very small pore sizes corresponding to 45–100 PPI and high porosity ($\varepsilon > 0.97$), and will be discussed in greater detail in Section 3.5. Lage et al. [53] conducted experiments on compressed foams at high velocities and found a cubic dependence of the pressure gradient with velocity in the turbulent regime. Recently, Paek et al. [32] reported their experimental results on high porosity metal foams ($0.89 < \varepsilon < 0.96$) with pore densities corresponding to 10, 20 and 40 PPI. They determined the value of f to be 0.105 and found K to be highest at $\varepsilon = 0.94$. However, no analysis or physical explanations were given for the results. In the following section, we report our experimental data on high porosity aluminum foams. The porosity range of our experimental samples is between 89% and 98% and PPIs are 5, 10, 20 and 40.

3.2. Experimental procedure

The experiments on the metal foam samples were conducted in the in-house wind tunnel (Fig. 3(b)). Aluminum metal foam samples (see Table 2) of size 62.5 mm × 43.75 mm × 192.5 mm, brazed to 9.375 mm thick aluminum skins of size 62.5 mm × 192.5 mm, were used in the experiments. The metal foam sample was placed in a ducted arrangement in the wind tunnel. Styrofoam insulation, which can be easily machined into the desired shape, was used to surround the samples to prevent air-bypass. Pressure taps were drilled into the aluminum skins at various axial locations of the metal foam and were connected to a pressure transducer (range 0–125 mm water column). The axial locations were chosen after allowing for a conservative developing length of 75 mm based on the estimate given in [2,54]. In addition, two pressure taps were provided at the inlet to and exit from the metal foam to measure the total pressure drop across the sample. An orifice plate (pipe dia-100 mm, and bore dia-36.25 mm) was used to monitor the flow rate. A digital thermometer was used to monitor the room temperature, and this value was used in the flow rate calculation. Pressure drop across the orifice plate was measured using a manometer for lower values (in the range 0–6.25 mm water column) and a pressure transducer for higher values (up to 25 mm water column). The pressure drop was converted into flow rate as specified in standard, ASME/ISO-5167-1:1991.

During a typical experiment run, the set-up as described above was first tested for leaks to ensure that the ducting was in place. Airflow rate through the metal foam was set at a desired value by adjusting the speed of the wind-tunnel fan. At each flow velocity, the pressure drop across various axial locations of the metal foam was measured. The pressure drop data collected during a typical experiment run were found to increase with L. However, the pressure gradient did not vary with the axial length. This was found to be true for all the samples tested, indicating that the flow was indeed fully developed. The pressure drop due to wall friction, estimated using the fully developed pipe flow correlation, was found to be less than 0.5% for the total pressure drop. This indicates that the measured pressure drop values are primarily due to the drag force exerted by the metal foam. Also note that more data points were acquired in the low velocity range in order to improve the

Table 2
Characteristics of the metal foam samples used for pressure drop experiments

Sample #	Porosity	PPI	d_f (m)	d_p	f	K ($\times 10^7$ m^2)
1	0.9726	5	0.0005	0.00402	0.097	2.7
2	0.9118	5	0.00055	0.0038	0.085	1.8
3	0.9486	10	0.0004	0.00313	0.097	1.2
4	0.9138	10	0.00045	0.00328	0.07	1.1
5	0.8991	10	0.00043	0.0032	0.068	0.94
6	0.9546	20	0.0003	0.0027	0.093	1.3
7	0.9245	20	0.00035	0.0029	0.104	1.1
8	0.9005	20	0.00035	0.00258	0.088	0.9
9	0.9659	40	0.0002	0.0019	0.101	0.55
10	0.9272	40	0.00025	0.00202	0.089	0.61
11	0.9132	40	0.00020	0.0018	0.084	0.53
12	0.971	5	0.00051	0.004	0.096	2.52
13	0.946	5	0.00047	0.0039	0.099	2.17
14	0.905	5	0.00049	0.0038	0.078	1.74
15	0.949	10	0.00037	0.0031	0.099	1.49
16	0.909	10	0.00038	0.00296	0.082	1.11
17	0.978	20	0.00038	0.0028	0.087	1.42
18	0.949	20	0.00032	0.0027	0.1	1.185
19	0.906	20	0.00034	0.0026	0.085	0.854
20	0.972	40	0.00023	0.0018	0.094	0.52
21	0.952	40	0.00024	0.00198	0.0976	0.562
22	0.937	40	0.00024	0.002	0.0899	0.568

accuracy in the estimation of K, as discussed in Section 3.4. For details of the measurement values, the reader is referred to Calmidi [6] and Bhattacharya [34].

3.3. Results

Noting that the flow is fully developed and the viscous effects are small, the momentum equation can be written as

$$\frac{\Delta p}{L} = au + bu^2. \tag{15}$$

A least-squares fit was performed to determine values of a and b. In all cases, the regression analysis yielded a fit with $R^2 > 99.9\%$ indicating that the quadratic relationship is valid. Comparing Eqs. (14) and (15), the values of K and f are

$$K = \frac{\mu}{a}, \quad f = \frac{b\sqrt{K}}{\rho}. \tag{16}$$

These values are listed in Table 2. We note that studies in the past [42,55,56] use a different method to estimate values of a and b. There, Eq. (15) is rewritten in the form $(1/u)(\Delta p/L) = a + bu$. Then, a best least-squares fit of $(1/u)(\Delta p/L)$ is obtained as a linear function of the velocity, and K and f are determined using the y-intercept and slope of this linear function. In principle, this procedure yields identical results to those obtained using parabolic fit, only if the quadratic relationship is exact. However, in reality this may not be so, and Antohe et al. [45] argue that the parabolic fit results in a higher error in the final values of K and f since it relies on extrapolation. However, in this study, we note that the difference in the values of K and f determined by the two methods was negligible, and the parabolic method was used throughout since it is more convenient.

3.4. Error analysis

The task of estimating uncertainties in the values of K and f is not straight-forward since it is not immediately clear how the uncertainties in the measurement of velocities and pressure drop propagate to affect the values of a and b in Eq. (15). It is obvious that the pressure gradient values are governed by a at lower velocities and by b at higher velocities. Following the method proposed by Antohe et al. [45], the uncertainties in the values of K and f were calculated for all the samples listed in Table 2, and were found to be in the range 5.2–13.9% for K, and 2.9–7.1% for f.

It is important to note that the uncertainty estimates obtained above by the method proposed by Antohe et al. [45] must be viewed with caution. The estimate is accurate only if experiments are conducted at sufficiently low and high velocities so that meaningful values of a and b can be determined. It is possible to drop some experimental points from the regression analysis and obtain smaller uncertainty estimates. For example, the uncertainty values associated with the estimation of K can be reduced if some of the low velocity points are not

considered. This is, however, undesirable since the low velocity points play a bigger role in the determination of K. Thus, in order to obtain meaningful uncertainty estimates for K and f, the experimental data set must contain measurements in the range of velocities where the Darcian component and the quadratic component of the pressure drop in Eq. (15) are of the same order of magnitude. For this reason, more data points were obtained in the low velocity range in our experiments as mentioned in Section 3.2.

3.5. Analytical models

3.5.1. Permeability

As stated in Section 3.1, Du Plessis et al. [52] presented a model for evaluating K and f for metal foams. That model was derived using experimental results from foam samples of very small pore sizes (45–100 PPI) and porosity of 0.973–0.978, and using water and glycerol as the fluid phase. Their expression for K is given by

$$\frac{K}{d^2} = \frac{\varepsilon^2}{36\chi(\chi-1)}, \tag{17}$$

where $d = \sqrt{\chi/(3\varepsilon)}d_p$, and χ, the tortuosity of the porous matrix, is defined as the ratio of the total winding path length available for flow in the representative unit cell of the porous medium to the basic stream wise length scale. Following Du Plessis [57] it is given by

$$\chi = \frac{\varepsilon d_p^2}{A_p}. \tag{18}$$

For their model consisting of three mutually orthogonal duct sections in a cubic unit cell [52,58], χ is expressed as

$$\frac{1}{\chi} = \frac{3}{4\varepsilon} + \frac{\sqrt{9-8\varepsilon}}{2\varepsilon}\cos\left\{\frac{4\pi}{3} + \frac{1}{3}\cos^{-1}\left[\frac{8\varepsilon^2 - 36\varepsilon + 27}{(9-8\varepsilon)^{3/2}}\right]\right\}. \tag{19}$$

When applied to our samples, this model was found to over-predict our experimental data for K by factors of 1.4–2.7 (see Fig. 5). The deviation is smaller at lower pore diameters or higher PPIs.

A closer look at the picture of the metal foam sample (60 PPI) in [52] (Fig. 1(a)) reveals that the lumping of metal at the intersection of two fibers, mentioned in Section 2.1, is absent. The presence of the lump of solid material at the intersection of two fibers in our samples introduces extra flow resistance by constricting the flow path and forcing the fluid to flow through more tortuous paths. As observed above, the deviation between the experimental data and model in [52] decreases as the pore diameter is decreased or PPI is increased. Qualitatively, as pore density (PPI) increases, the number of fibers increases, and so does the flow resistance due to the fibers. As a result, at higher PPIs, the relative contribution due to the lumping at the intersections in obstructing the flow is reduced. This accounts for the lower deviation from the model in [52] at higher PPIs.

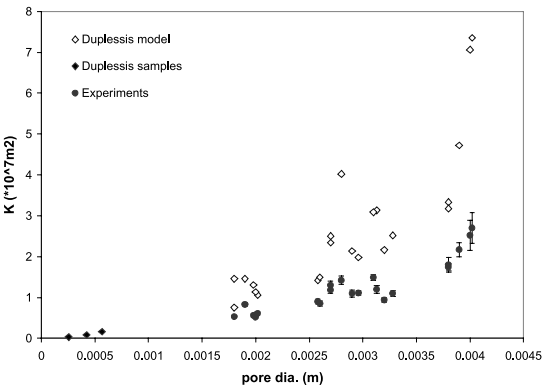

Fig. 5. Experiments vs. model of Du Plessis et al. [52] for permeability K.

The main conclusion from the above argument is that Eq. (19) is not applicable for determining χ for our metal foam samples. To derive an appropriate expression we recall that $\chi = \varepsilon d_p^2/A_p$, where $A_p = (\pi/4)(d_p^2 - d_f^2)$. Substituting d_f/d_p from Eq. (4), we get

$$\frac{1}{\chi} = \frac{\pi}{4\varepsilon}\left\{1 - \left(1.18\sqrt{\frac{(1-\varepsilon)}{3\pi}}\frac{1}{G}\right)^2\right\}. \tag{20}$$

The model predictions using Eqs. (17) and (20) along with experimental data are plotted in Fig. 6(a). The agreement between the two over a wide range of pore diameter is fairly good. Thus, unlike the existing model reported in [52] which is accurate only at high pore densities (PPIs), the new model can be applied over a wider range of porosities and pore densities (PPIs) for determining K of metal foams.

We also note that contrary to the experimental data of Paek et al. [32], our results do not show any optimum ε for which K is maximum. For a given pore diameter, K is found to increase with ε (see Fig. 6(b)). This seems physically consistent since for a given pore density (PPI), the fiber diameter decreases (though very slowly) with increase in porosity, see Table 2. As a result the open cross-sectional area available for fluid flow in a pore increases, which reduces flow resistance. Hence K is expected to increase with porosity. In the limiting case when ε approaches 1, the value of K should approach infinity (since the porous medium ceases to exist and hence, the Darcy term should go to zero). As a result, we do not expect any optimum ε for maximum K.

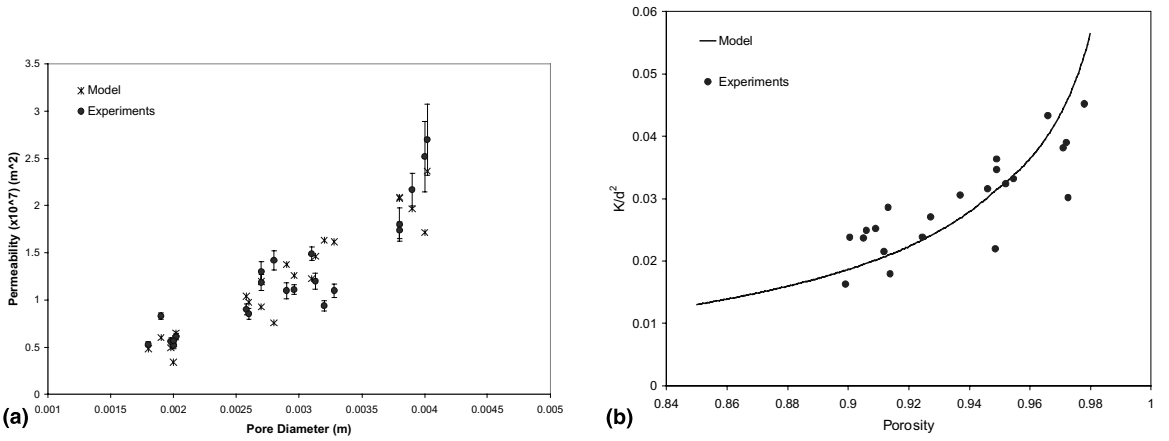

Fig. 6. (a) Permeability (K): experiments vs. model (Eqs. (17) and (20)). (b) Permeability (K) as a function of porosity: experiments vs. model (Eqs. (17) and (20)).

3.5.2. Inertial coefficient

Du Plessis et al. [52] had also presented a model for the inertial coefficient which is reproduced below in Eq. (21):

$$f = \frac{2.05\chi(\chi-1)}{\varepsilon^2(3-\chi)}\frac{\sqrt{K}}{d^2}. \tag{21}$$

When applied to our samples, the values of inertial coefficients are found to be 30–70% off except for samples in the porosity range of 95% or higher (see Fig. 7(a)). Noting that the model was based on samples with $\varepsilon > 97\%$, the suggestion is that the model may be valid only in the high porosity range. Further, a closer look into Eq. (21) shows f to monotonically decrease with ε. Again this is true for our experimental data only in the range of $\varepsilon > 0.97$. For lower porosities, i.e. in the range $0.85 < \varepsilon < 0.97$, our data show that f actually increases with increase in ε. This contrasting behavior can be explained as follows.

The inertial coefficient, f, is a measure of the drag experienced during fluid flow past the fibers. Hence it is expected to strongly depend on the shape of the fiber cross-section. As noted in Section 1 [6,7], and also revealed by our photographs taken under a microscope (see Fig. 7(b)), the cross-section of the fiber changes from a circle to a concave triangle in the range of $0.85 < \varepsilon < 0.97$. In this range of ε, it is this change in shape of the cross-section that causes f to increase with increase in ε. The model derived in [52] is for fiber cross-sections of concave triangle only and does not take into account the variation in cross-section for $0.85 < \varepsilon < 0.97$. To overcome this drawback, we propose a new model for f based on the theory for flow over bluff bodies, for the two different porosity domains, viz. $0.85 < \varepsilon < 0.97$ (Domain I) and $\varepsilon > 0.97$ (Domain II). Noting the correspondence between pressure drop for flow in metal foams to that over bluff bodies one can write

$$\frac{fL}{\sqrt{K}}\rho v^2 \sim \frac{C_D(\varepsilon)}{2}\rho v^2 \quad \text{or} \quad f \sim \frac{C_D(\varepsilon)}{2}\frac{\sqrt{K}}{L}, \tag{22}$$

where the length L in the flow direction can be scaled with the fiber diameter d_f for flow over a bluff body. Eq. (22) can, therefore, be rewritten as

$$f = M\frac{C_D(\varepsilon)}{2}\frac{\sqrt{K}}{d_f} = M\frac{C_D(\varepsilon)}{2}\frac{\sqrt{K}}{d_p}\left(\frac{d_f}{d_p}\right)^{-1}. \tag{23}$$

Substituting Eqs. (17) and (4) in Eq. (23), we get

$$\begin{aligned} f &= M\frac{C_D(\varepsilon)}{2}\frac{\varepsilon}{\sqrt{36\chi(\chi-1)}}\sqrt{\frac{\chi}{3\varepsilon}}\left(1.18\sqrt{\frac{(1-\varepsilon)}{3\pi}}\frac{1}{G}\right)^{-1} \\ &= M\frac{C_D(\varepsilon)}{12}\sqrt{\frac{\varepsilon}{3(\chi-1)}}\left(1.18\sqrt{\frac{(1-\varepsilon)}{3\pi}}\frac{1}{G}\right)^{-1}. \end{aligned} \tag{24}$$

The unknowns in Eq. (24) are the constant M and the drag coefficient $C_D(\varepsilon)$ for the different fiber cross-sections. These can be determined as follows.

Domain I ($0.85 < \varepsilon < 0.97$).

Recalling that the fiber cross-sections are circles and equilateral triangles for $\varepsilon = 0.85$ and $\varepsilon = 0.94$, respectively, the values of C_D for $\varepsilon = 0.85$ and $\varepsilon = 0.94$ in Eq. (24) can be taken from standard values known for flows over bluff bodies. Using references [59,60] these values are 1.2 and 1.75, respectively. The constant M is then found to be equal to 0.095. Eq. (24) hence reduces to

$$f = 0.095\frac{C_D(\varepsilon)}{12}\sqrt{\frac{\varepsilon}{3(\chi-1)}}\left(1.18\sqrt{\frac{(1-\varepsilon)}{3\pi}}\frac{1}{G}\right)^{-1}. \tag{25}$$

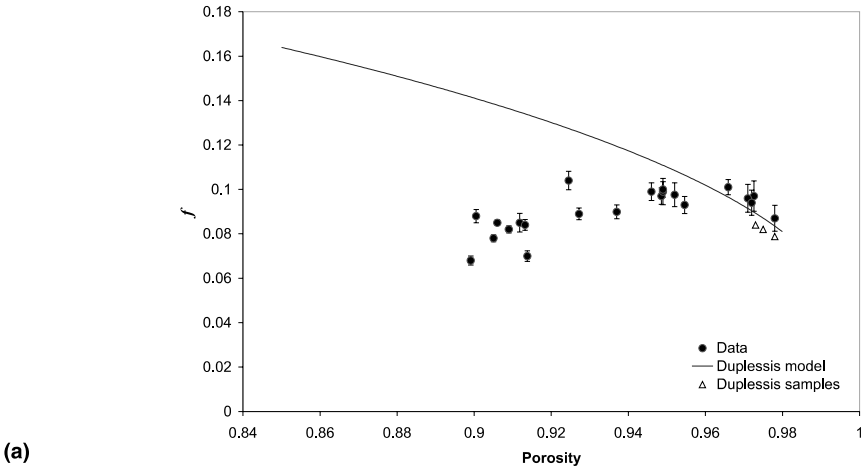

(a)

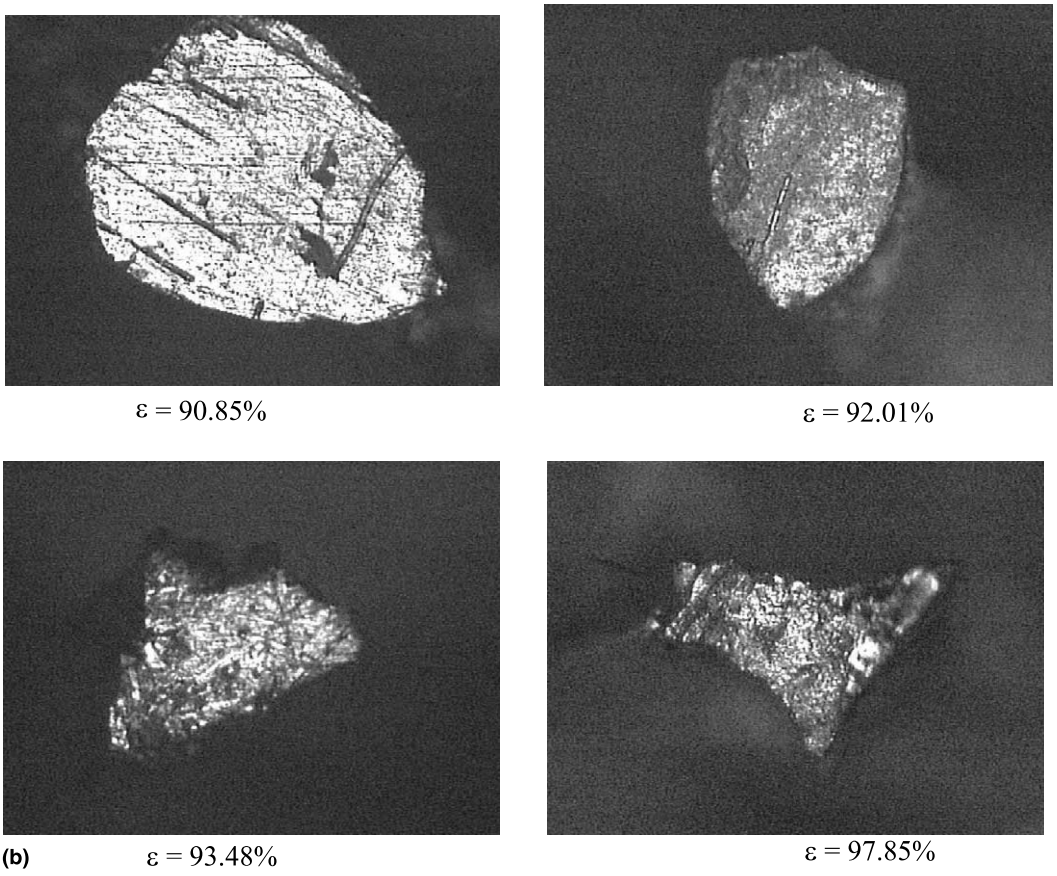

(b)

Fig. 7. (a) Experiments vs. model of Du Plessis et al. [52] for inertial coefficient, f. (b) Photographs of the fiber cross-sections at different porosities taken under a microscope.

Eq. (25) is a general expression, which can be used to determine C_D for a given cross-section (or porosity) if the experimental value for f is known. Alternatively, it can be used to determine f if C_D is known at that porosity. For example, at $\varepsilon = 0.9659$ the experimental value of f is 0.101 (see Table 2). The value of C_D at that porosity (where the shape of the fiber cross-section is most likely to be a concave triangle) can, therefore, be

calculated to be 1.85. For other cross-sections with varying shape in the domain $0.85 < \varepsilon < 0.97$, we propose

$$C_D(\varepsilon) = C_D(0.85)S = C_D(0.85)G^n, \tag{26}$$

where S is the shape function which in turn is related to the geometric function G. The relation satisfies the boundary condition of $C_D(0.85) = 1.2$ since the geometric function $G = 1$ for $\varepsilon = 85\%$. Using the known values for $C_D(\varepsilon)$ at $\varepsilon = 0.85$, 0.94 and 0.965, the index n is determined to be -0.8, so that the final expression for the inertial coefficient for $0.85 < \varepsilon < 0.97$ becomes

$$f = 0.095\frac{C_D(0.85)}{12}G^{-0.8}\sqrt{\frac{\varepsilon}{3(\chi-1)}}\left(1.18\sqrt{\frac{(1-\varepsilon)}{3\pi}}\frac{1}{G}\right)^{-1}, \tag{27}$$

where $C_D(0.85) = 1.2$.

Eq. (27) is plotted along with the experimental data in Fig. 8(a). As seen the agreement of the data with the model is excellent. The drag coefficient becomes larger as the fiber cross-section changes from a circle to a concave triangle. As a result, f increases with ε. The attendant decrease in fiber diameter (and hence projected area) for a given pore density, on the other hand, is very small (see Table 2). As mentioned earlier, Du Plessis et al. [52] did not take into account this variation in fiber cross-section with porosity. Hence their f values at lower porosities were much higher than the experimental data. When the drag coefficient correction is added to their model, the predicted values decrease significantly as shown in Fig. 8(a). The agreement with the experimental data now improves with the maximum deviation being less than 20%.

Domain II ($\varepsilon \geqslant 0.97$).

For porosities greater than 97%, the fiber cross-section is assumed to retain its shape of a concave triangle. Thus with further increase in ε, $C_D(\varepsilon)$ remains unchanged. Hence the inertial coefficient, f can be obtained by substituting G by $G(\varepsilon = 0.97) = 0.5831$ in Eq. (27). Fig. 8(b) shows the agreement of the model with our experimental data in this porosity range. Consistent with the results of Du Plessis et al. [52] f decreases with ε in this porosity range. This is because beyond $\varepsilon = 97\%$, even though the drag coefficient remains constant, the fiber diameter becomes smaller (reduction in projected area) thereby decreasing the net form drag.

4. Summary

Analytical and experimental investigations were conducted for the determination of the effective thermal conductivity, k_e, permeability K, and the inertial coefficient f of metal foam samples of different porosities and pore sizes. For the determination of k_e, a theoretical model was formulated, which represents the metal foam structure by a two-dimensional hexagonal array where the fibers form the sides of the hexagons. The lump of metal at the intersection of two fibers seen in commercially available metal foam samples was represented as an intersection of circular cross-section. The analysis and experiments showed that the effective thermal conductivity of the foam depends strongly on the porosity and the ratio of the cross-sections of the fiber and the intersection. However no systematic dependence was found on pore density. Experimental data with aluminum and RVC foams, using air and water as fluid media were used to validate the theoretical model and were found to be in excellent agreement with the model predictions. Finally, a simple, closed-form empirical correlation was also derived for estimating the effective thermal conductivity in terms of the porosity, and the solid and fluid conductivities. Analytical models were also proposed for the determination of K and f for flow

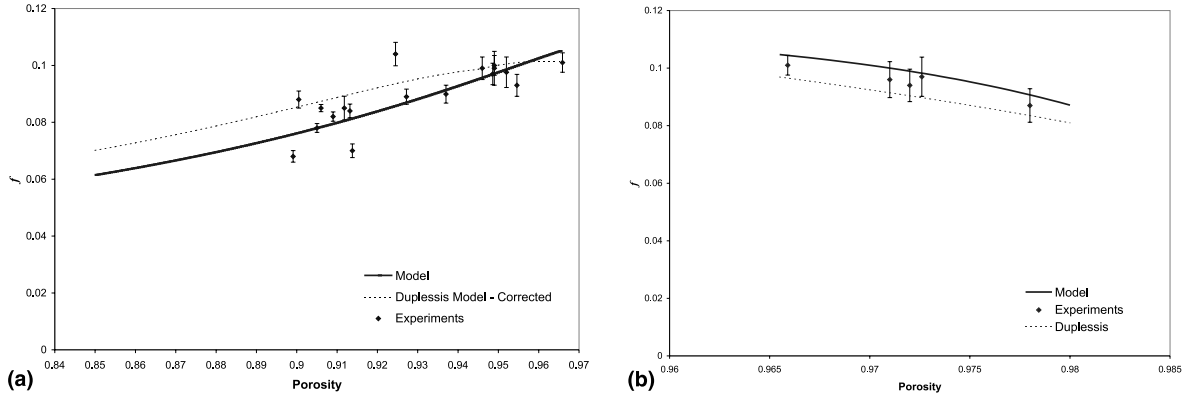

Fig. 8. (a) Inertial coefficient (f): experiments vs. model (Eq. (27)) for $0.85 < \varepsilon < 0.97$. (b) Inertial coefficient (f): experiments vs. model (Eq. (27)) for $\varepsilon > 0.97$.

through metal foams. For K, the existing model of Du Plessis et al. [52] was modified to incorporate our correction for the tortuosity for our metal foam samples. A new inertial coefficient model was proposed based on the theory of form drag for flow over bluff bodies that takes into account the variation of the shape of fiber cross-sections with porosity. The f model proposed by Du Plessis et al. [52], originally valid only in the high porosity domain ($\varepsilon \geqslant 0.97$), was also modified to account for the variation in fiber cross-section and was found to give much better agreements with the experimental data, even in the lower porosity range of $0.85 < \varepsilon < 0.97$.

Acknowledgements

The authors gratefully acknowledge the financial support received from CAMPmode, The Center for Advanced Manufacturing and Packaging of microwave, optical, and digital electronics at the University of Colorado. The authors would also like to thank Mr. Bryan Leyda of ERG (Energy Research and Generation), for providing the samples used in the experimental studies.

References

[1] F.A.L. Dullien, Porous Media: Fluid Transport and Pore Structure, Academic Press, New York, 1979.
[2] M. Kaviany, Principles of Heat Transfer in Porous Media, Springer, New York, 1991.
[3] D.B. Ingham, I. Pop (Eds.), Transport Phenomena in Porous Media, Pergamon Press, Danvers, 1998.
[4] D.A. Nield, A. Bejan, Convection in Porous Media, second ed., Springer, New York, 1999.
[5] K. Vafai (Ed.), Handbook of Porous Media, Marcel Dekker, New York, 2000.
[6] V.V. Calmidi, Transport phenomena in high porosity metal foams, Ph.D. Thesis, University of Colorado, Boulder, CO, 1998.
[7] B. Leyda, Personal Communications, ERG Aerospace, 2000.
[8] L. Rayleigh, On the influence of obstacles arranged in rectangular order upon the properties of a medium, Philos. Mag. 34 (1892) 481–502.
[9] M.I. Aivazov, I.A. Domashnev, Influence of porosity on the conductivity of hot pressed titanium specimens, Sov. Powder Metall. Met. Ceram. 7 (1968) 708–710.
[10] P. Zehner, E.U. Schlunder, Thermal conductivity of granular materials at moderate temperatures, Chem.-Ing.-Tech. 42 (1970) 933–941.
[11] G.W. Milton, Bounds on the elastic and transport properties of two-component composites, J. Mech. Phys. Solids 30 (3) (1982) 177–191.
[12] Z. Hashin, Analysis of composite materials – a survey, ASME J. Appl. Mech. 50 (1983) 481–505.
[13] I. Nozad, R.G. Carbonell, S. Whitaker, Heat conduction in multi-phase systems I: theory and experiments for two-phase systems, Chem. Eng. Sci. 40 (1985) 843–855.
[14] P.A. Smith, S. Torquato, Computer simulation results for bounds on the effective conductivity of porous media, J. Appl. Phys. 65 (3) (1989) 893–900.
[15] I.C. Kim, S. Torquato, Determination of the effective conductivity of heterogeneous media by Brownian motion simulation, J. Appl. Phys. 68 (8) (1990) 3892–3903.
[16] L.S. Verma, A.K. Shrotriya, R. Singh, D.R. Chaudhary, Prediction and measurement of effective thermal conductivity of three-phase systems, J. Phys. D 24 (1991) 1515–1526.
[17] M. Sahraoui, M. Kaviany, Slip and no-slip temperature boundary conditions at interface of porous, plain media: conduction, Int. J. Heat Mass Transfer 36 (4) (1993) 1019–1033.
[18] T.H. Bauer, A general approach toward the thermal conductivity of porous media, Int. J. Heat Mass Transfer 36 (17) (1993) 4181–4191.
[19] C.L. Tien, K. Vafai, Statistical bounds for the effective thermal conductivity of microsphere and fibrous insulation, AIAA Progress Ser. 65 (1979) 135–148.
[20] C.T. Hsu, P. Cheng, K.W. Wong, Modified Zehner–Schlunder models for stagnant thermal conductivity of porous media, Int. J. Heat Mass Transfer 37 (17) (1994) 2751–2759.
[21] C.T. Hsu, P. Cheng, K.W. Wong, A lumped-parameter model for stagnant thermal conductivity of spatially periodic porous media, ASME J. Heat Transfer 117 (1995) 264–269.
[22] S. Whitaker, The Method of Volume Averaging, Kluwer Academic Publishers, Boston, 1999.
[23] P. Cheng, C.T. Hsu, Heat conduction, in: D.B. Ingham, I. Pop (Eds.), Transport Phenomena in Porous Media, Pergamon Press, UK, 1998, pp. 57–76.
[24] C.T. Hsu, Heat conduction in porous media, in: K. Vafai (Ed.), Handbook of Porous Media, Marcel Dekker, New York, 2000, pp. 171–200.
[25] W.J. Mantle, W.S. Chang, Effective thermal conductivity of sintered metal fibers, AIAA J. Thermophys. Heat Transfer 5 (1991) 545–549.
[26] G.N. Dul'nev, B.L. Muratova, Thermal conductivity of fibrous systems, J. Eng. Phys. 14 (1968) 29–35.
[27] E.G. Alexander, Structure–property relationships in heat pipe wicking materials, Ph.D. Thesis, North Carolina State University, Raleigh, NC, 1972.
[28] J.C.Y. Koh, A. Fortini, Prediction of thermal conductivity and electrical resistivity of porous metalic materials, Int. J. Heat Mass Transfer 6 (1973) 2013–2021.
[29] M.G. Semena, V.K. Zaripov, Influence of the diameter and length on material heat transfer of metal fiber wicks of heat pipes, Tepleonergetika 24 (1977) 82–84.
[30] J. Januszewski, M.I. Khokhar, A.S. Majumdar, Thermal conductivity of some porous metals, Lett. Heat Mass Transfer 4 (1977) 417–423.
[31] V.V. Calmidi, R.L. Mahajan, The effective thermal conductivity of high porosity metal foams, ASME J. Heat Transfer 121 (1999) 466–471.

[32] J.W. Paek, B.H. Kang, S.Y. Kim, J.M. Hyun, Effective thermal conductivity and permeability of aluminum foam materials, Int. J. Thermophys. 21 (2) (2000) 453–464.
[33] K. Boomsma, D. Poulikakos, On the effective thermal conductivity of a three dimensionally structured fluid-saturated metal foam, Int. J. Heat Mass Transfer 44 (2001) 827–836.
[34] A. Bhattacharya, Thermophysical properties and convective transport in metal foam and finned metal foam heat sinks, Ph.D. Thesis, University of Colorado, Boulder, CO, 2001.
[35] A. Bhattacharya, V.V. Calmidi, R.L. Mahajan, An analytical–experimental study for the determination of the thermal conductivity of high porosity metal foams, in: R.M. Sullivan, N.J. Salamon, M. Keyhani, S. White, Application of Porous Media Methods for Engineered Materials, AMD-Vol. 233, 1999, pp. 13–20.
[36] MARC™ User Manuals, MARC Analysis Research Corporation, Palo Alto, CA, 1999.
[37] D.A. Zumbrunnen, R. Viskanta, F.P. Incropera, Heat transfer through granular beds at high temperature, Warme- Stoffubertrag. 18 (1984) 221–226.
[38] D.A. Zumbrunnen, R. Viskanta, F.P. Incropera, Heat transfer through porous solids with complex internal geometries, Int. J. Heat Mass Transfer 29 (1986) 275–284.
[39] T.R. Taylor, An Introduction to Error Analysis – The Study of Uncertainties in Physical Measurements, University Science Book, Mill Valley, 1980.
[40] H. Darcy, Les Fontaines Publiques de la ville de Dijon, Dalmont, Paris, 1856.
[41] P. Forchheimer, Wasserbewegung durch boden, VDI Z. 45 (1901) 1782–1788.
[42] G.S. Beavers, E.M. Sparrow, Non-darcy flow through fibrous porous media, ASME J. Appl. Mech. 36 (4) (1969) 711–714.
[43] K. Vafai, C.L. Tien, Boundary and inertia effects on convective mass transfer in porous media, Int. J. Heat Mass Transfer 25 (8) (1982) 1183–1190.
[44] D.D. Joseph, D.A. Nield, G. Papanicolaou, Nonlinear equation governing flow in a saturated porous medium, Water Resour. Res. 18 (1982) 1049–1052.
[45] B. Antohe, J.L. Lage, D.C. Price, R.M. Weber, Experimental determination of permeability and inertial coefficients of mechanically compressed aluminum metal layers, ASME J. Fluids Eng. 119 (1997) 404–412.
[46] S. Ergun, Fluid flow through packed column, Chem. Eng. Prog. 48 (2) (1952) 89–94.
[47] S. Irmay, On the theoretical derivation of Darcy and Forcheimer formula, Trans. Am. Geograph. Union 39 (4) (1958) 702–707.
[48] H. Rumpf, A.R. Gupta, Einflusse der porositat and kongroß enverteilung im widerstandsgesetz der porenstromung, Chem.-Ing.-Tech. 43 (1971) 367–375.
[49] I.F. Macdonald, M.S. El-Sayed, K. Mow, F.A.L. Dullien, Flow through porous media: the Ergun equation revisited, Ind. Chem. Fund. 18 (1979) 199–208.
[50] R.M. Fand, B.Y.K. Kim, A.C.C. Lam, R.T. Phan, Resistance to the flow of fluids through simple and complex porous media whose matrices are composed of randomly packed spheres, ASME J. Fluids Eng. 109 (1987) 268–274.
[51] I. Kececioglu, Y. Jiang, Flow through porous media of packed spheres saturated with water, ASME J. Fluids Eng. 116 (1994) 164–170.
[52] P. Du Plessis, A. Montillet, J. Comiti, J. Legrand, Pressure drop prediction for flow through high porosity metallic foams, Chem. Eng. Sci. 49 (1994) 3545–3553.
[53] J.L. Lage, B. Antohe, D.A. Nield, Two types of nonlinear pressure-drop versus flow-rate relation observed for saturated porous media, ASME J. Fluids Eng. 119 (1997) 700–706.
[54] K. Vafai, C.L. Tien, Boundary and inertia effects on flow and heat transfer in porous media, Int. J. Heat Mass Transfer 24 (1981) 195–203.
[55] M.L. Hunt, C.L. Tien, Effects of thermal dispersion on forced convection in fibrous media, Int. J. Heat Mass Transfer 31 (1988) 301–309.
[56] G.J. Hwang, C.H. Chao, Heat transfer measurements and analysis for sintered porous channels, ASME J. Heat Transfer 117 (1994) 725–732.
[57] J.P. Du Plessis, Pore scale modeling for flow through different types of porous environments, in: M. Quintard, M. Todorovic (Eds.), Heat and Mass Transfer in Porous Media, Elsevier, Amsterdam, 1992, pp. 249–262.
[58] J.P. Du Plessis, J.H. Masliyah, Mathematical modeling of flow through consolidated isotropic porous media, Transp. Porous Media 3 (1988) 145–161.
[59] S.F. Hoerner, Fluid Dynamic Drag, Midland Park, NJ, 1965.
[60] B.R. Munson, D.F. Young, T.H. Okiishi, Fundamentals of Fluid Mechanics, fourth ed., Wiley, New York, 1998.